M Ű E G Y E T E M 1 7 8 2
BUDAPEST UNIVERSITY OF TECHNOLOGY AND ECONOMICS
DEPARTMENT OF CONSTRUCTION MATERIALS AND TECHNOLOGY

THERMAL IMAGER APPLICATIONS DURING TENSILE STRENGTH TEST OF REINFORCEMENT BARS

TDK 2021

GODWIN EMMANUEL BANDAWA

SUPERVISORS:
DR. NAGY BALÁZS
DR SÁNDOR SÓLYOM

Budapest, 2021.10.31

Contents

List of figures

List of Tables

ABSTRACT

Reinforcement bars which are used widely in construction typically in concrete to withstand tension stresses, reduce cracking and brittle failure. Therefore, it is highly important that these rebars meet the requirement of tensile strength and fit into limit state designs. Understanding the mechanical behavior of rebars is important in building constructions and optimizations. Mechanical stress induces temperature change in the reinforcement bars depending on their physical parameters, such as thermal diffusivity. This effect can be observed using a thermal imager, which have suitable field of view, resolution and thermal sensitivity, as well as capable of recording fully radiometric videos. In published research, mostly steel reinforced bars were investigated using thermal imagers, but fiber reinforced polymers have not yet. Hence, this paper is to explore the viability of the use of a thermal imager in the tensile strength test for multiple types of reinforcement bars. In this research an experimental investigation on the thermal properties and behavior of steel and fiber reinforced polymer bar during a tensile test with a thermal imager is conducted. The aim of the investigation is to compare the radiometric datasets with the stress-strain diagram of the specimen during the test and analyze the performance of different reinforcement bars with different diameters, as well as specimens under different load conditions. The performed tests show whether the thermal imager is applicable to predict the failure and its location regarding different kinds of reinforcement bars.

KEYWORDS

Tensile strength, Thermal imaging, Reinforcement steel, Fiber reinforced polymer (FRP) bar

COMMON ABBREVIATIONS USED IN THIS PAPER

FRP – Fibre Reinforcement Polymer

GFRP – Glass Fibre Reinforcement Polymer

IR – Infrared

IRT – Infrared Thermography

Rebar – Reinforcement Bar

UTM – Universal Testing Machine

1. INTRODUCTION

Thermography is the most popular technique used to measure temperature differences of surfaces by infrared wave emission using thermal camera. These cameras provide a means for temperature measurement in building constructions from the inside as well as from the outside. Thus heat bridges can be detected. It has been shown that infrared thermography is applicable for several other application [1].

In construction technology thermal imaging is a powerful tool to investigate structural condition and structural elements and as well be used for damage assessment. It is highly efficient, non-destructive and non-contact method that enables rapid investigations even though this technology is not widely explored by the Architecture Engineering and Construction (AEC) professionals. With improved software the data obtained from the thermal camera in form of radiometric videos or images can be analyzed concisely and visualized in form of thermograms and meaningful graphs or charts.

Poor construction materials have accounted for a lot of avoidable deaths and loss of valuable resources hence it is necessary to evaluate the performance of building materials in order improve construction safety requirements. Reinforcement bars are important component in several aspects of construction project especially in reinforced concrete structures.

This study aims to analyze the thermal properties of reinforcement bars during tensile strength test monitoring the heating and cooling process in real time, the tensile strength. Tensile strength derived from factors such as fibre strength, fibre length, and bond strength of adhesives of building components, and structural elements. The test may be used to deduce information about these factors, especially when used as a tensile strength index. Critical consideration of the conventional quantities obtained from the tensile test reveals their limitations for design purposes, especially where notch-fatigue effects predominate. Against such notch-fatigue the importance of high work-hardening capacity in a metal is emphasized, and its relation to tensile elongation behavior outlined [2].

Steel and fibre reinforced polymer bar are the primary specimen for this experiments, FRP bars are composites, made by embedding fibres into a polymeric resin. Fibres are the load bearing components, while the resin protects the fibres and transfers the stresses. Commonly used fibres are aramid (A), basalt (B), carbon (C) and glass (G), the latter is the most widely used for structural engineering. The most often applied resins are thermoset (epoxy, polyester and vinyl ester) [3]. FRP is a relatively new class of non-corrosive, high-strength, lightweight material,

have emerged over the past approximately 20-30 years as practical materials for a number of structural engineering applications [4]. Due to their low density, FRP are increasingly used than the more conventional materials (steel, aluminum, alloys…) in order to design lighter products especially in the aeronautics sector [5].

Steel-reinforced concrete is one of the most widely used construction materials around the world based on its high tensile and compressive strength provided by the combination of concrete and steel rebar. However, the long-term performance of steel reinforced concrete is reduced because of the corrosion of steel; and high costs of inspection, maintenance, and restoration of corroded steel reinforcements are required [6]. During the last few decades, for providing the flexural and shear reinforcements, the employment of FRP rebars in reinforced concrete members is increasing. Some investigations have been carried out to examine the performance of FRP rebars as longitudinal and transverse reinforcements in compressive and flexural members which depicted a better response of FRP rebars in these members [7].

2. METHODOLOGY

In order to achieve the purpose of this study the research design is illustrated in Figure 1, a literature review was carried out based on selected keyword from all relevant, high-quality individual studies addressing one or more aspects of the study.

Figure 1. *Research design/procedure*

The specimens used were prepared, the steel rebars and the FRP bars were made ready and available for the experiment, attaching testing grip to the FRP bar. Furthermore, acquiring a standard tripod in order to achieve the right field of view and stability of the camera during recording capturing the temperature for every pixel of the image is important.

Furthermore, the tensile test experimentation was conducted under required standards while observing the thermal properties with the imager, the detailed steps for setting the camera are further elaborated in the chapter 4 of this study.

Results from the experiment were exported into readable file formats via a software known as IRSoft, and analyzed with Microsoft Excel to plot curves and calculate characteristics values. The thermal camera can record a fully radiometric video It offers the possibility of analyzing saved videos and sequences in the clearly structured software Testo IRSoft, saving individual images either as a thermal image of a BMP-file, JPEG-file or a PNG-file.

3. LITERATURE REVIEW

“Infrared thermography (IRT) is a non-contact, non-invasive methodology which allows for detection of thermal energy that is radiated from objects in the infrared band of the electromagnetic spectrum, for conversion of such energy into a visible image (such as a surface temperature map). This feature represents a great potential to be exploited in a vast variety of fields from aerospace to civil engineering, to medicine, to agriculture, etc.”[8]. Composite materials such as Fibre Reinforcement Polymer (FRP) are broadly used in high performance applications due to their widely known advantages: principally high specific strength and corrosion resistance but it is worth to mention about their price and accessibility [9].

The concept of emissivity of the surface of a material is its effectiveness in emitting energy as thermal radiation. Quantitatively, emissivity is the ratio of the thermal radiation from a surface to the radiation from an ideal black surface at the same temperature as given by the Stefan–Boltzmann law.

3.1 Emission, reflection, transmission

Emissivity (ε) is a measure of the ability of a material to emit (give off) infrared radiation. Emissivity is defined as the ratio of the energy radiated from a material's surface to that radiated from a perfect emitter, known as a blackbody, at the same temperature and wavelength and under the same viewing conditions. It is a dimensionless number between 0 (for a perfect reflector) and 1 (for a perfect emitter) [10].

Reflectance (ρ)

Reflectance (ρ) is a measure of the ability of a material to reflect infrared radiation. ρ depends on the surface properties, the temperature and the type of material.

Transmittance (τ)

Transmittance (τ) is a measure of the ability of a material to transmit (allow through) infrared radiation, transmittance t of a medium is defined by the ratio of transmitted radiant power to incident radiant power [11].

Base on Kirchhoff’s rules for Conservation of energy principle for radiation, the infrared radiation recorded by the thermal imager consists of the radiation emitted by the measuring object, the reflection of ambient radiation and the transmission of radiation through the measuring object.

It is represented with the formula:

$$\varepsilon + \rho + \tau = 1 \quad (1)$$

3.2 Correlation between emission and reflection

1. Measuring objects with high emissivity ($\varepsilon \geq 0.8$): have low reflectance (ρ): $\rho = 1 - \varepsilon$
2. Measuring objects with medium emissivity ($0.6 < \varepsilon < 0.8$): have medium reflectance (ρ): $\rho = 1 - \varepsilon$
3. Measuring objects with low emissivity ($\varepsilon \leq 0.6$): have high reflectance (ρ): $\rho = 1 - \varepsilon$

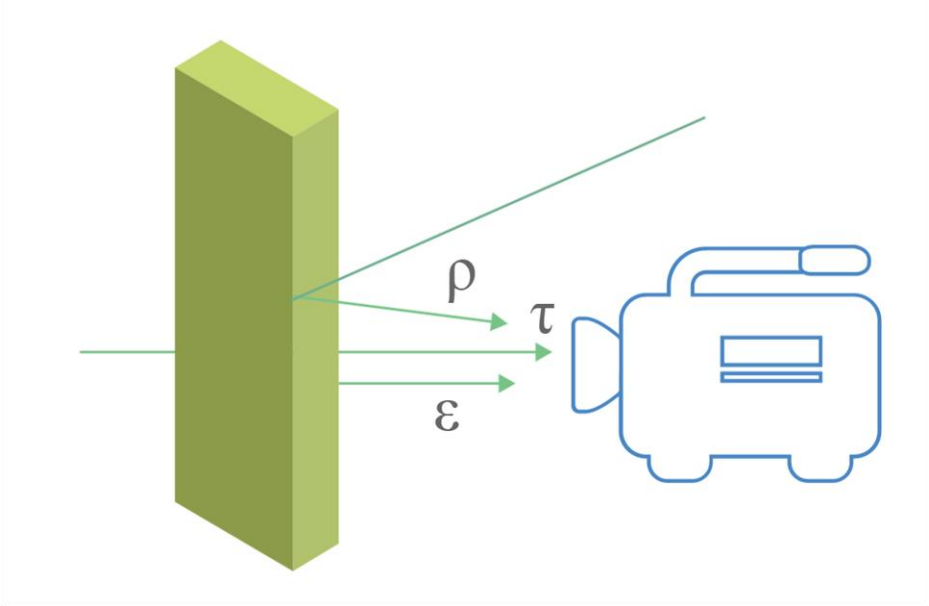

Figure 2. *Emission, reflection and transmission*

Figure 2 illustrates the correlation between emissivity, reflectance and transmission while undertaking infrared thermography measurements, all of the above depends not only on the material but also on the nature of the surface.

4. MATERIALS AND TESTING METHOD

4.1 Experimental Concept, Active vs passive thermography

There are two different applicable approaches regarding IR thermography, i.e. the passive and the active approach. In passive thermography, the features of interest are naturally at a higher or

lower temperature than the background. Abnormal temperature profiles indicate a potential problem, and a key term is temperature difference with respect to a reference, often referred to as

ΔT value or hot spot. Generally, passive thermography is rather qualitative since the goal is simply to detect anomalies. On the other hand, in active thermography, it is necessary to conduct some energy in the specimen inspected in order to obtain significant temperature differences witnessing the presence of subsurface anomalies [12]. The active approach is necessary in many cases given that the inspected parts are usually in equilibrium with the surroundings which is employed in this investigation.

4.2 Thermal camera

Thermal cameras see the world very differently to how the human eye does. Our eyes rely on visible light passing into them to construct images using feedback from our brains in complex patterns, but thermal imaging devices use infrared (IR) light instead to create an image. IR light is completely invisible to the human eye; this type of light is outside the spectrum of light that our eyes can detect, but is all around us on a daily basis. Thermal camera use complex algorithms and thermal lenses to pick up on this heat distribution and relay what they see as a thermal image [13]. In this study a Testo 885-2 (Figure 3) a professional thermal imager was used with a resolution of 320 x 240 pixels, upgradable to 640 x 480 pixels with SuperResolution, thermal sensitivity < 30 mK.

Figure 3. *testo 885-2 used in the experiment*

The technical details of the camera are provided in Table 1 [14]:

***Table 1**. specifications of testo 885-2 thermal camera*

Operating temperature	-15 to +50 °C
Spectral range	7.5 to 14 µm
Infrared resolution	320 x 240 pixels
Thermal sensitivity	< 30 mK at +30 °C
Field of view	30° x 23° (Standard lens), 25° x 19° (25° lens), 11° x 9° (Telephoto)
Minimum focus distance	0.1 m (Standard lens), 0.2 m (25° lens), 0.5 m (Telephoto lens)
Geometric resolution (IFOV)	1.7 mrad (Standard lens), 1.36 mrad (25° lens), 0.6 mrad (Telephoto lens)
SuperResolution (Pixel)	640 x 480 pixels
SuperResolution (IFOV)	1.06 mrad (Standard lens), 0.85 mrad (25° lens), 0.38 mrad (Telephoto lens)
Image refresh rate	33 Hz
Focus	auto / manual
Emissivity	0.01; 1
Measuring range	-30 to +100°C; 0 to +350 °C (switchable); 0 to +650 °C (switchable)
High temperature measuring	+350 ... +1200 °C (not in connection with the telephoto lens)
Analysis function	up to 10 measurement points, Hot/Cold Spot Recognition, up to 5 x area measurement (min/max & average), Isotherm and alarm values

4.3 Test specimen and method

Most structural engineering problems could be formulated as optimization problems that achieve optimum structural performance whilst satisfying conflicting design constraints[15]. For the purpose of this study steel reinforced bars and FRP bar were investigated, the type of FRP bar used in this study is called a Glass Fibre reinforced polymer bar (GFRP bars), having free length of 44-48 cm during the tensile tests. The bars were anchored to grooved steel pipes in both end to compensate for local failure, slippage, and low gripping capacity of the bars. as

shown in Figure 4, the GFRP bars were provided by two different manufacturers. The steel bars have free length of 35-40 cm, for the purpose of this study three different diameters were chosen and are tested.

Figure 4. *prepared specimen of the GFRP*

The FRP bars as shown in Figure 4 were fabricated by Hughes Brothers, Inc., (the lower three bars in Figure 4), and the others pieces by Perfa Komopozity, Inc (the upper three bars in Figure 4). the tensile test and specimen preparation were conducted base on relevant standards and requirement ISO/FDIS 10406-1:2014(E) [16] for the FRP bars and ISO 15630-1:2019 [17] for steel rebars. The tensile tests were performed in a displacement control manner at a low rate of 10 mm/min and 50 mm/min to obtain the post-peak tensile behavior of the bars. Figure 5 below shows the experimental setup during the tensile testing.

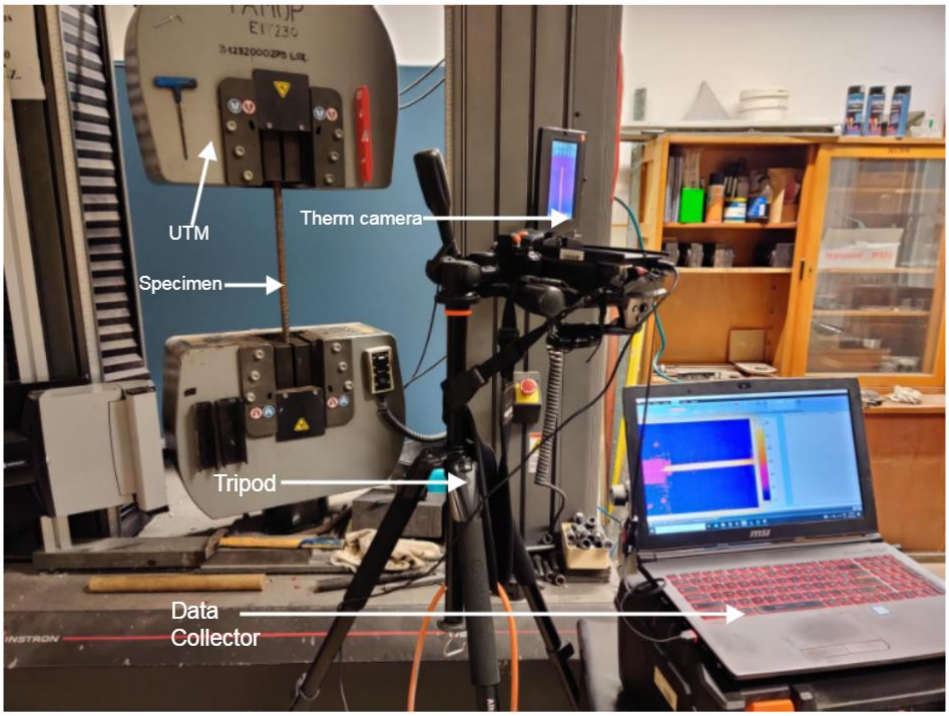

Figure 5. *experimental setup of the tensile testing*

4.4 Methodological analysis

After the tensile test, results are exported in Excel file format including the loaded forces, head displacements and time. The thermal camera captures the thermal behavior of the observed specimen and it is set to record in a radiometric video format. The producers of the camera has provided a software called IRSoft, a widely used, transparently structured and user-friendly PC software that enables comprehensive computer analysis of thermal images. For example, different emission factors for different materials can be corrected for each image area, or even for individual pixels. To display critical temperatures, the software can be used to highlight whether the limits have been exceeded, along with pixels in a specific temperature range. In addition, a measuring point can be specified without a quantitative limit, hot / cold points can be defined, and text comments can be added to the thermal image via the Thermal Imager App [18].Subsequently, the recorded value of the various points are exported in an Excel file format. Eighteen steel rebars specimens and six GFRP bar**s** were involved in the experimental program. Table 2 and 3 shows the specifications of both types of bar specimens.

Table 2. *Specifications of steel rebars*

Order number the Experiment	**Diameter of steel bar (mm)**	**Loading rate (mm/min)**
1	16	10
2	16	10
3	16	10
4	16	50
5	16	50
6	16	50
7	25	50
8	25	50
9	25	50
10	25	10
11	25	10
12	25	10
13	8	50
14	8	50
15	8	50
16	8	10
17	8	10
18	8	10

Table 3*. Specifications of FRP bars*

Experiment Number	**Diameter (mm)**	**Loading Rate (mm/min)**
1	10	10
2	10	10
3	10	10
4	10	10
5	10	10
6	10	10

4.5 Test setup

The camera is calibrated before the test to record accurate measurement of the bar, the surface temperature of the bar is measured with a contact thermometer and then the emissivity of the camera is set, the reflected temperature (RTC) can be set individually to compensate the effect of the ambient temperature. Additionally, to minimize the effect of any possible suspended particles in the air the camera is placed at a horizontal distance of 83 cm between the lens and the specimen. To get a clear image and video the focus is adjusted correctly on the area relevant to the measurement. Figure 6 illustrates the calibration process using a contact thermometer on the specimen.

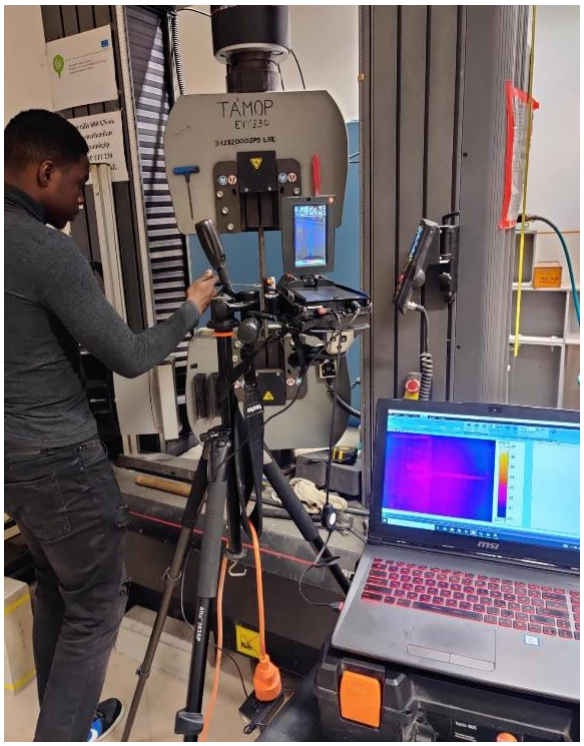

Figure 6. *calibration process of the camera.*

During this process conditions such as sunshine or reflection from the sky are neglected because it is conducted in a closed laboratory, also the experiments was conducted in late autumn hence heating systems were used in the building this implies that surrounding temperature remains constant, the RTC is set to be 2°C lower than the room temperature. The emissivity is set for the tested materials, with a Testo 905-T2 contact thermometer the tested specimen is measured to obtain its temperature at specific point, subsequently the emissivity of the camera is adjusted until the observed temperature from the camera correlates with the values from the thermometer, this values however should fall within plausible range for the material.

5. RESULTS AND DISCUSSION

This chapters presents the results of the mechanical tests with temperature differences. The results include the ultimate tensile strength of the steel and GFRP bars and the temperature elevation of the bar.

5.1 Emissivity value

After calibrating the camera and adjusting all necessary settings, the emissivity of the steel bar is set between 0.5 and 0.6, and the emissivity of the GFRP is 0.8; this value depends on how rusty the surfaces of the rebars are. Rustier bars had higher emissivity, than polished ones.

5.2 Steel specimen

This study uses an active thermography approach hence It was then possible to establish a specific relationship between tensile test results and the thermal behavior of the hot spot of the bar.

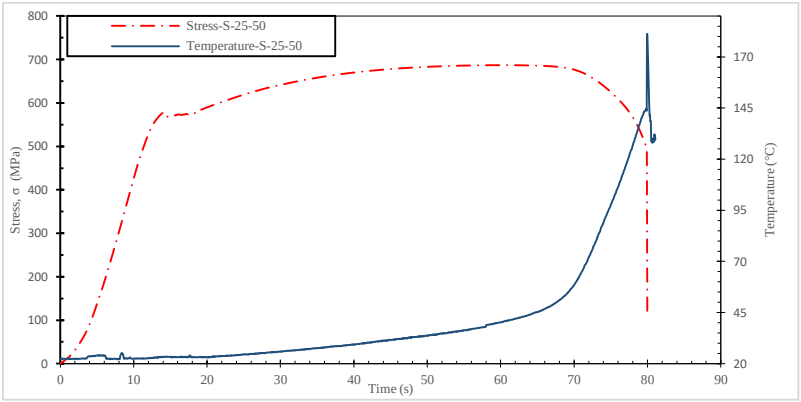

(7a)

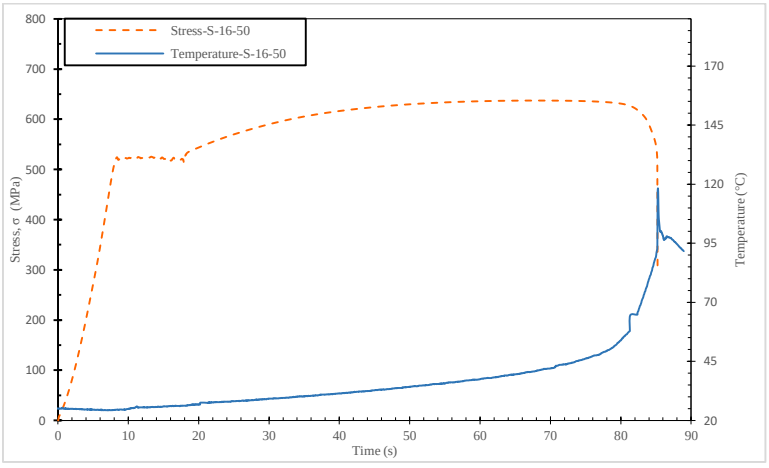

(7b)

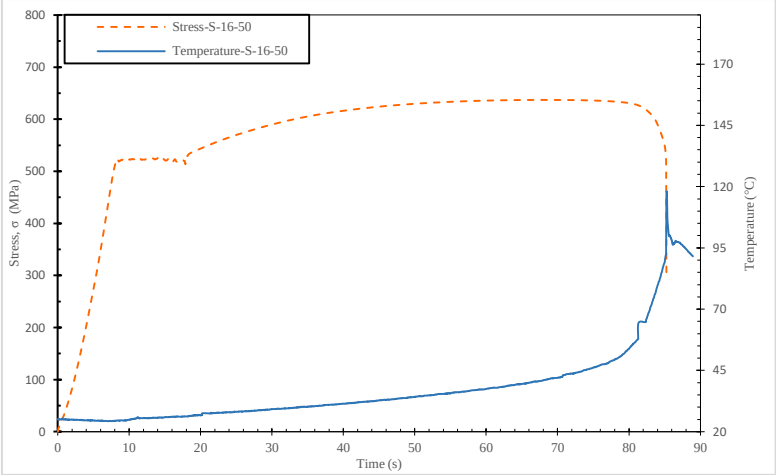

(7c)

Figure 7. *Tensile test (steel) at 50mm/min displacement rate. Stress-time (left), temperature-time(right)*

Figure 7 shows the stress on the left and the recorded temperature on the right ordinate axis for the steel bar, the curve labels are denoted as *Stress-S-08-50*, where "S" stands for Steel, the second number of the symbol *08* stands for the diameter of the specimen and the last *50* for the loading rate (in mm/min) in the examined graph. The same indication is applied for the temperature as well. The temperature changes at a slow rate and rapidly increase just before the point of failure. The highest temperature occurred in the bar with the largest diameter. Figure 8 shows the stress-strain curve with respect to the change in temperature.

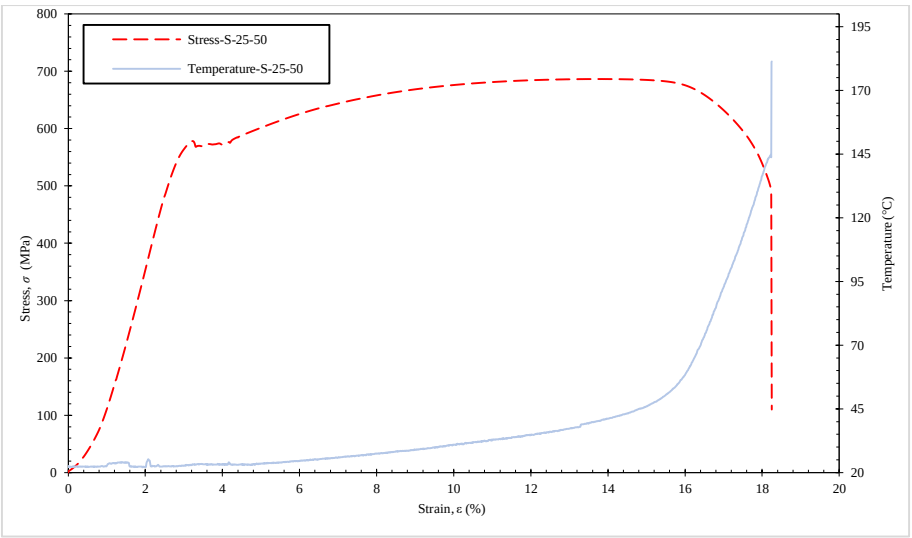

(8a)

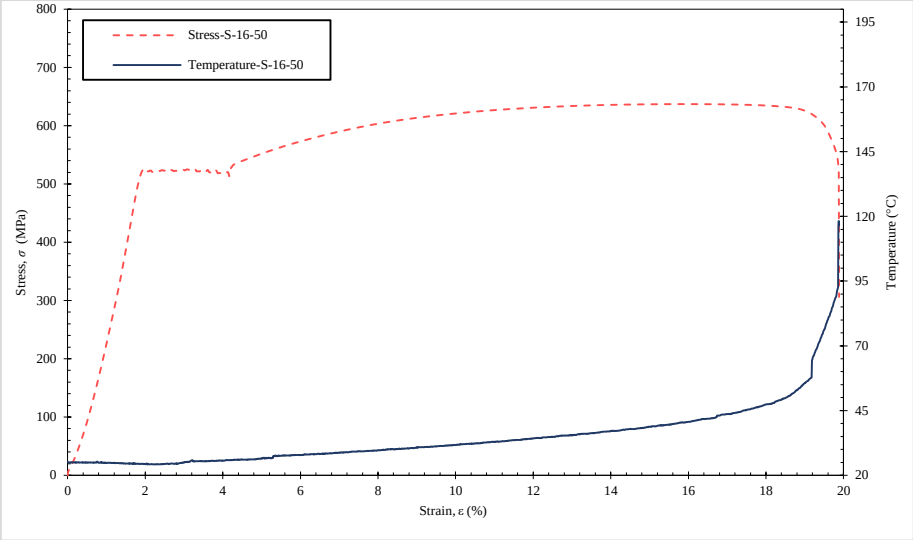

(8b)

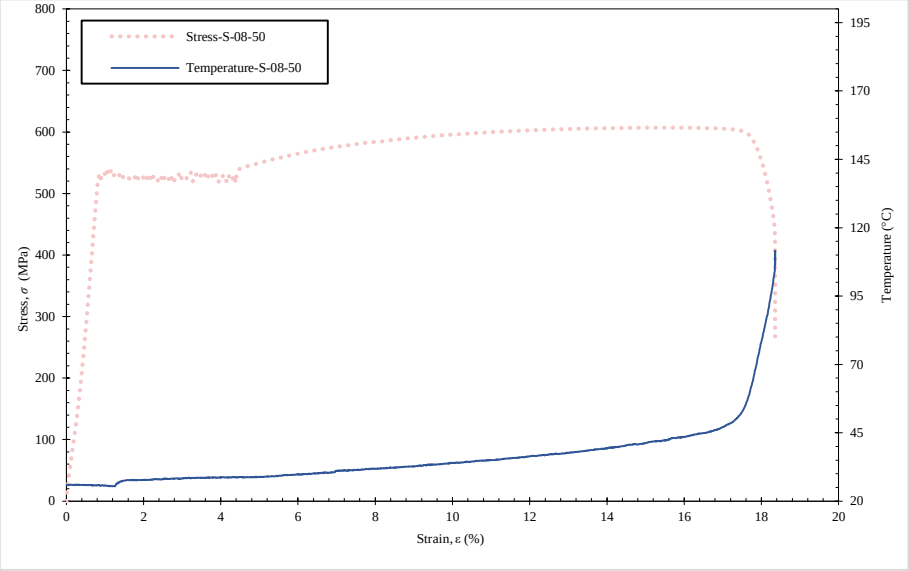

(8C)

Figure 8*. tensile test (steel) at 50mm/min displacement rate. Stress-strain (left), temperature-strain(right)*

The analysis was conducted based on the two different loading rates for the steel specimens test. Therefore, Figure 10 show the information from the steel specimen based on the 10 mm/min displacement rate the labels for the line are the same as in Figure 7 and 8.

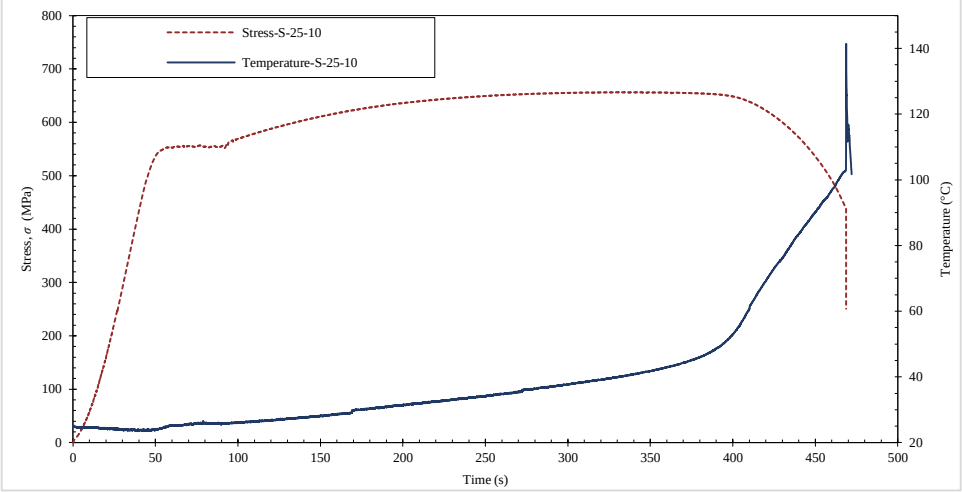

(9a)

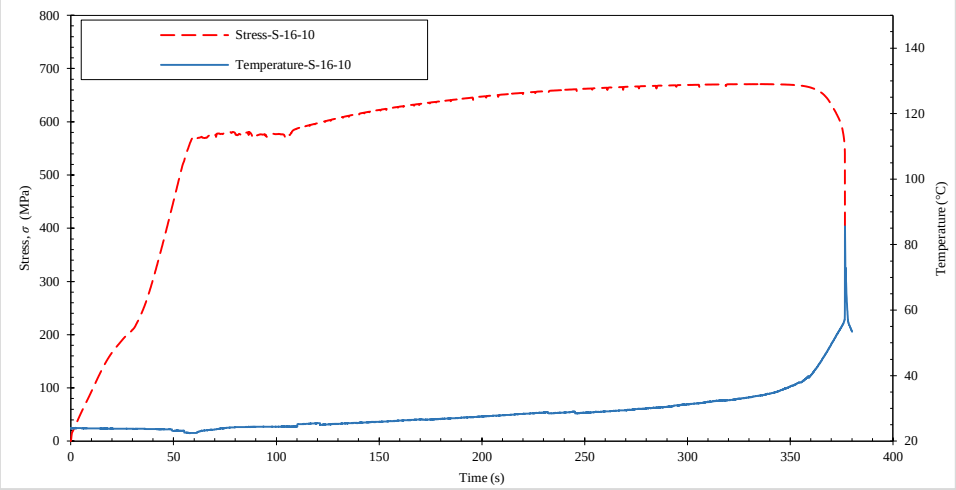

(9b)

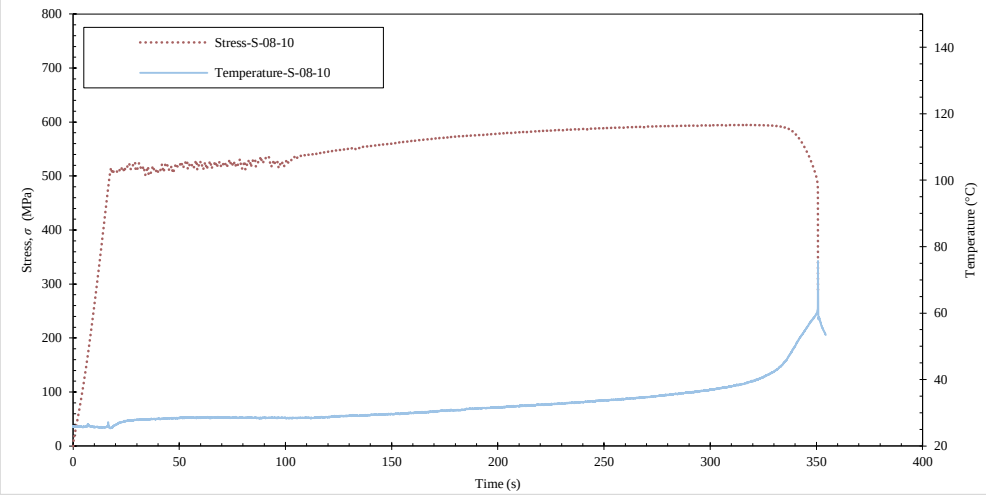

(9c)

***Figure 9**. Tensile test (steel) at 10mm/min displacement rate. Stress-time (left), temperature-time(right)*

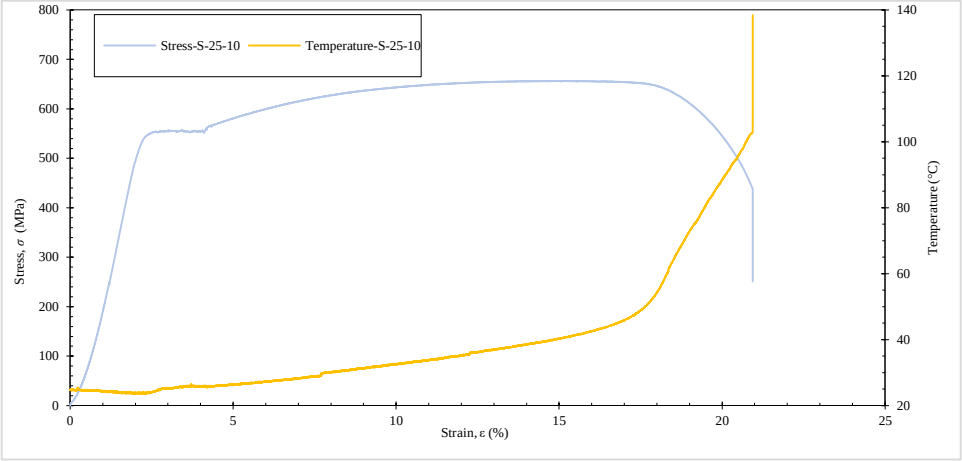

(10a)

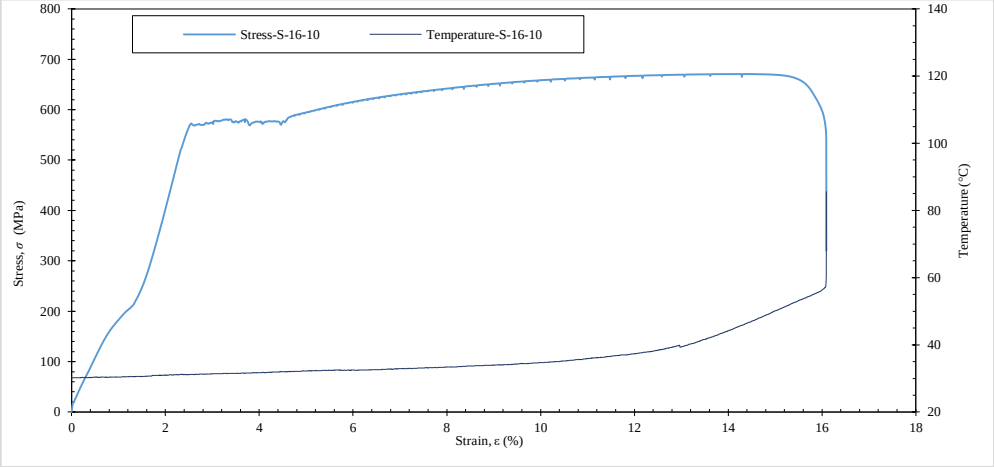

(10b)

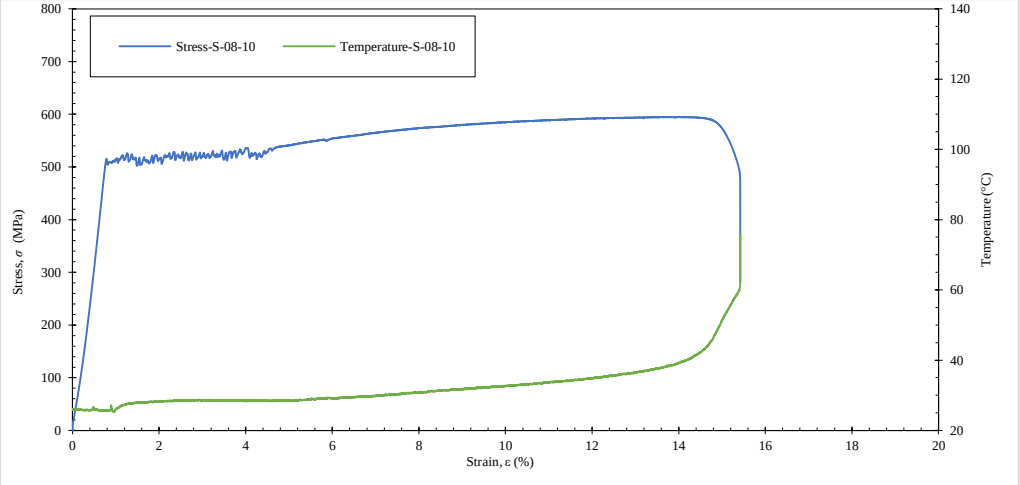

(10c)

Figure 10. *tensile test (steel) at 10mm/min displacement rate. Stress-strain (left), temperature-stress(right)*

In Figure 9, it shows that the thermal behavior is the same regardless of the loading rate however it shows higher thermal characteristics in experiment with higher displacement rate. Figure 10 shows the stress-strain diagram with respect to the temperature. From the steel experiments the temperature increases at elevated stress level, the temperature is increased up to 181.3°C.

5.3 GFRP specimen

The failure mode of the GFRP and steel rebars differs (Figure 11), the fibres in the GFRP bars fails suddenly in an irregular pattern, as shown in Figure 12. This in turn makes it impossible to measure a specific hotspot within the length of the rebar. Moreover, the highest temperature of the fibres of the bar heat up along the whole length of the bar as shown in the Figure 13. Temperature of the FRP was not as high as the steel bar, in order to measure temperature variation of the FRP bar a measuring point was added at the midpoint of the bar.

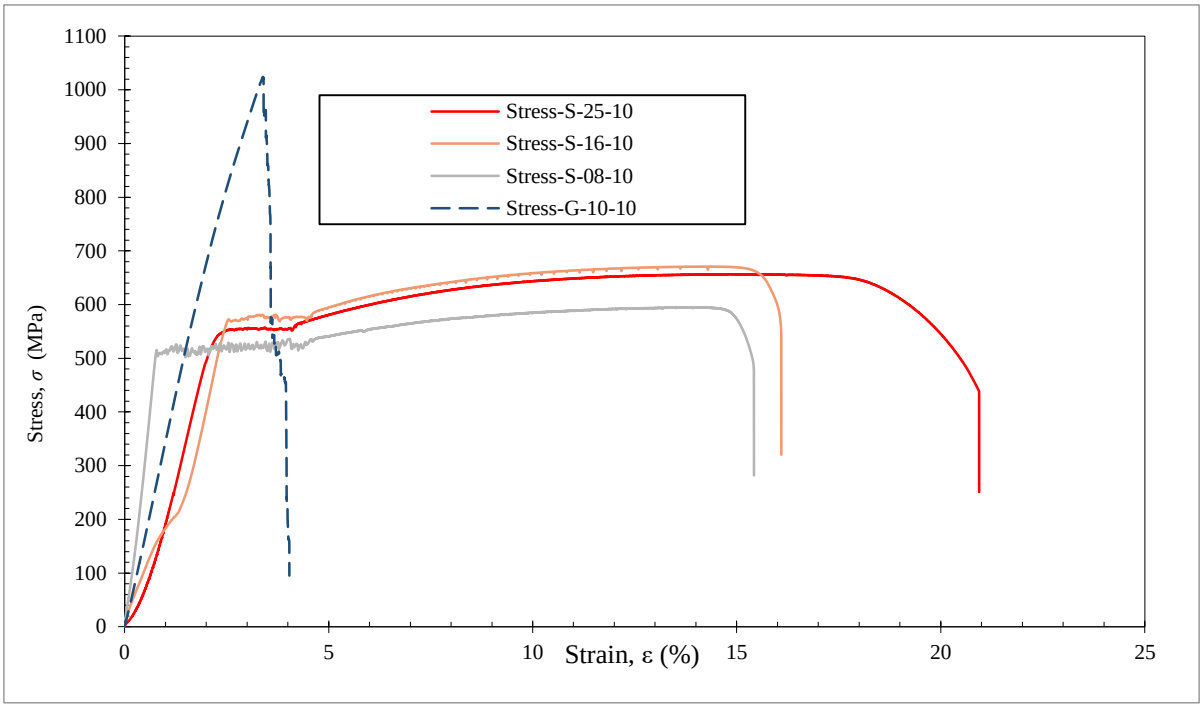

Figure 11. *Stress-strain curve for steel and GFRP bars*

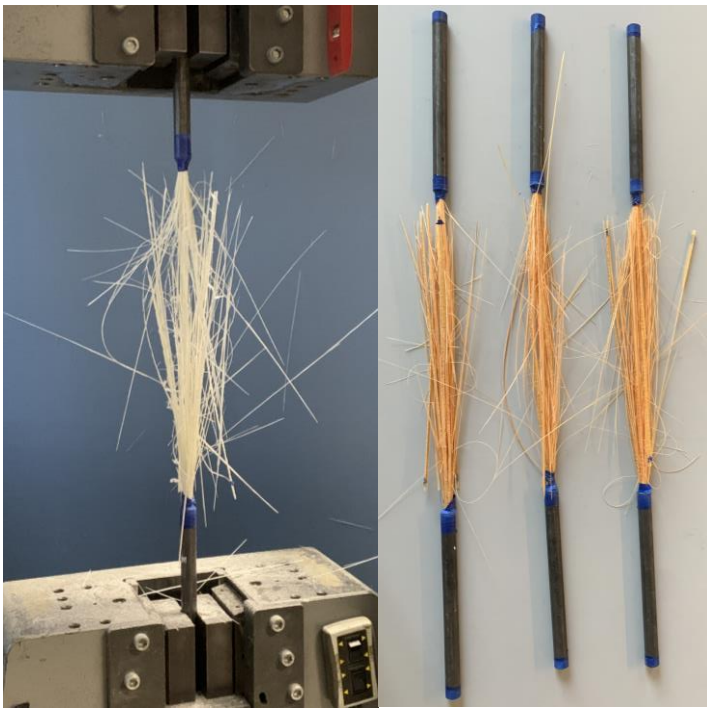

Figure 12. *Failure pattern of GFRP*

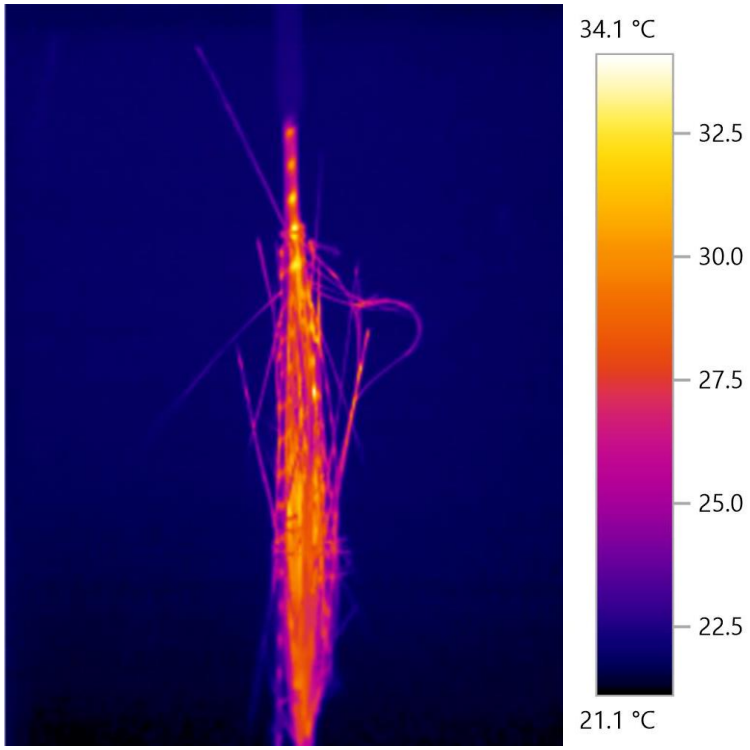

Figure 13. *The heated fibres of GFRP bar at failure*

Figure 14 relates the stress-strain curve with temperature change rise of GFRP bar surface. The curves are labeled as *Stress-G3-10-10*, the variables "G" stands for GFRP, the second number

"10" for the diameter of the specimen and the last "10" for the loading rate (in mm/min) in the examined graph. Thermal changes appear to be static until point of failure where it goes up to maximum recorded temperature of 63.8°C.

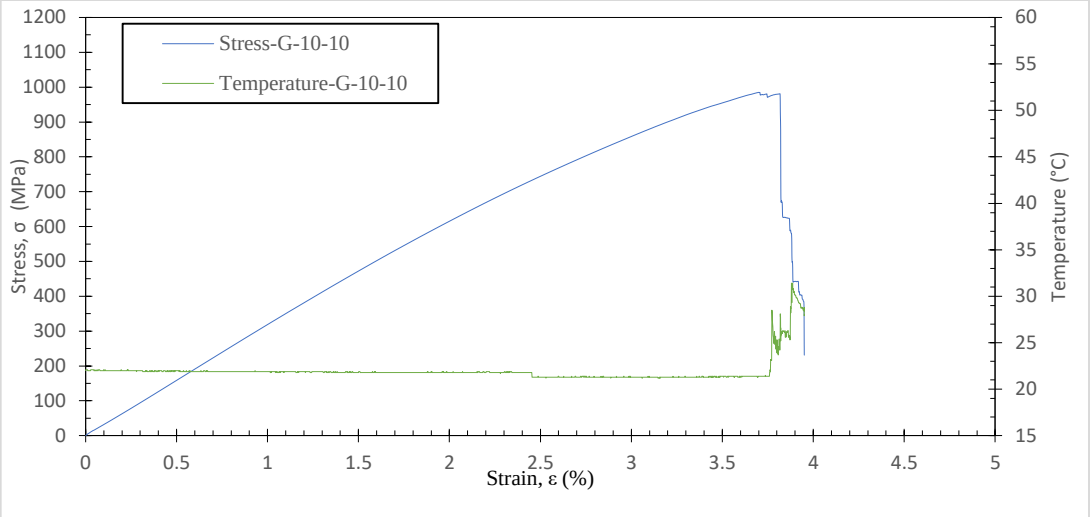

Figure 14. *tensile test (FRP) at 10mm/min displacement rate. Stress-strain (left), temperature-strain(right)*

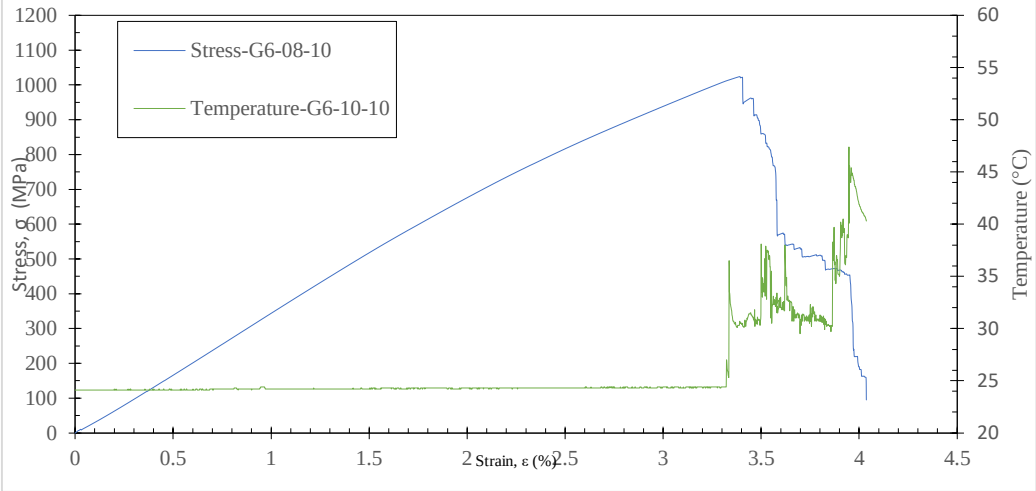

Figure 15. *tensile test (FRP) at 10mm/min displacement rate. Stress-strain (left), temperature-strain(right)*

In figure 14 measuring point was used in order to observe the thermal behavior. From the software a measuring point is inserted at the midpoint of the bar while in figure 15 the temperature scale is plotted with the hotspot, the hottest point of the bar this curve is relative to the stress-strain curve of the FRP bar.

Summary of the highest temperature from the experiment is shown in table 4:

Table 4. *Summary of highest temperature*

Diameter (mm)	**Type**	**Temperature (°C)**	**Displacement rate (mm/min)**
25	Steel	181.3	50
25	Steel	141.4	10
16	Steel	94.2	10
16	Steel	124.4	50
08	Steel	82.3	10
08	Steel	114.6	50
10	GFRP	47.7	10

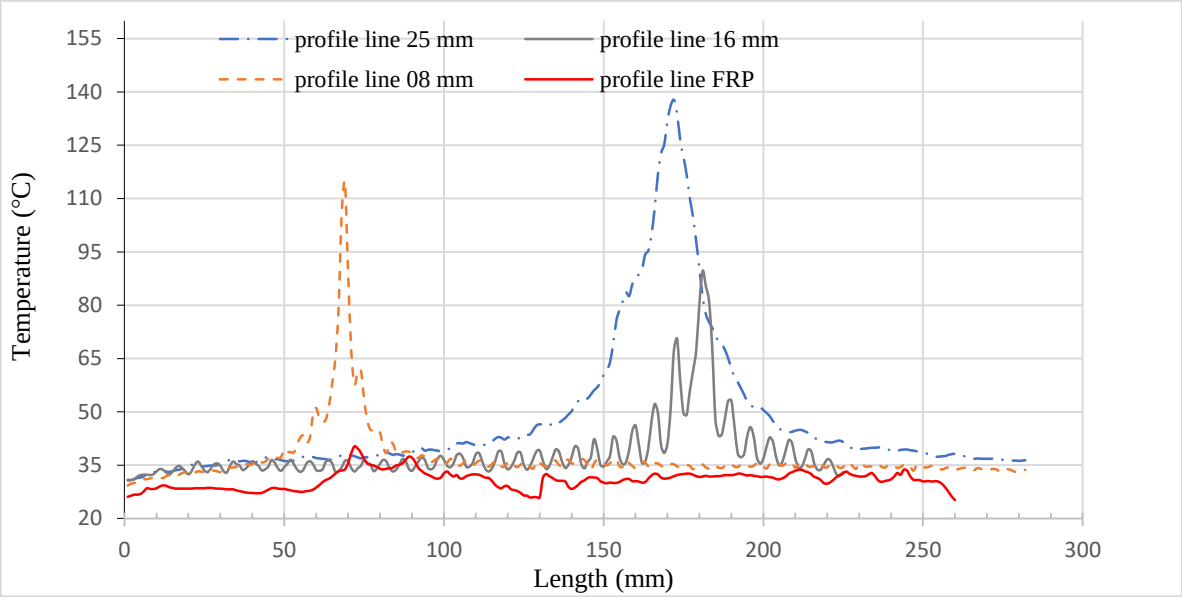

Figure 16. *profile line of the bars at failure*

Figure 16 shows the temperature of the bars at the point of failure, each line represents a steel bar (different diameter) and the GFRP bar. The steel bars show similar behaviors, and the highest temperature value indicates where the failure occurred the other length of the bar have much lower values. In the GFRP bar the temperature curve cannot indicate the point of failure however it shows that the bar heat up at along the whole length of the fibres with slight temperature differences. Higher temperatures are attained in bars with larger diameter and

higher loading rate. Table 4 summarize the highest temperatures attained in the experiments. Figure 16 and 17 displays the profile line of the rebar matched with the deformed bar.

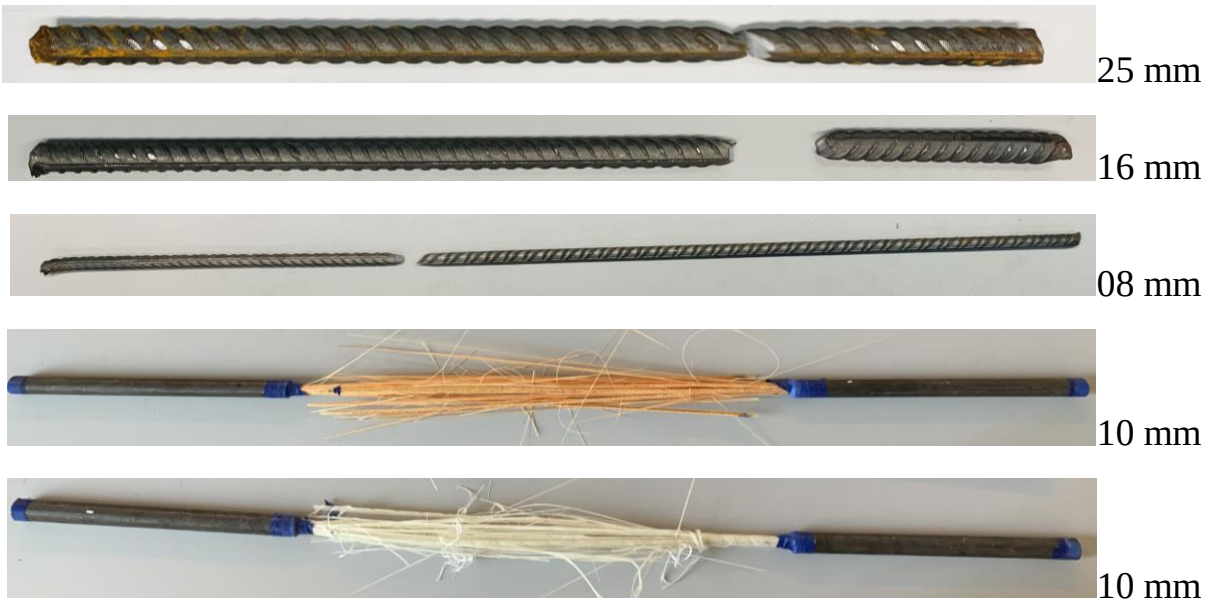

***Figure 17**. position of failure for different bar diameters*

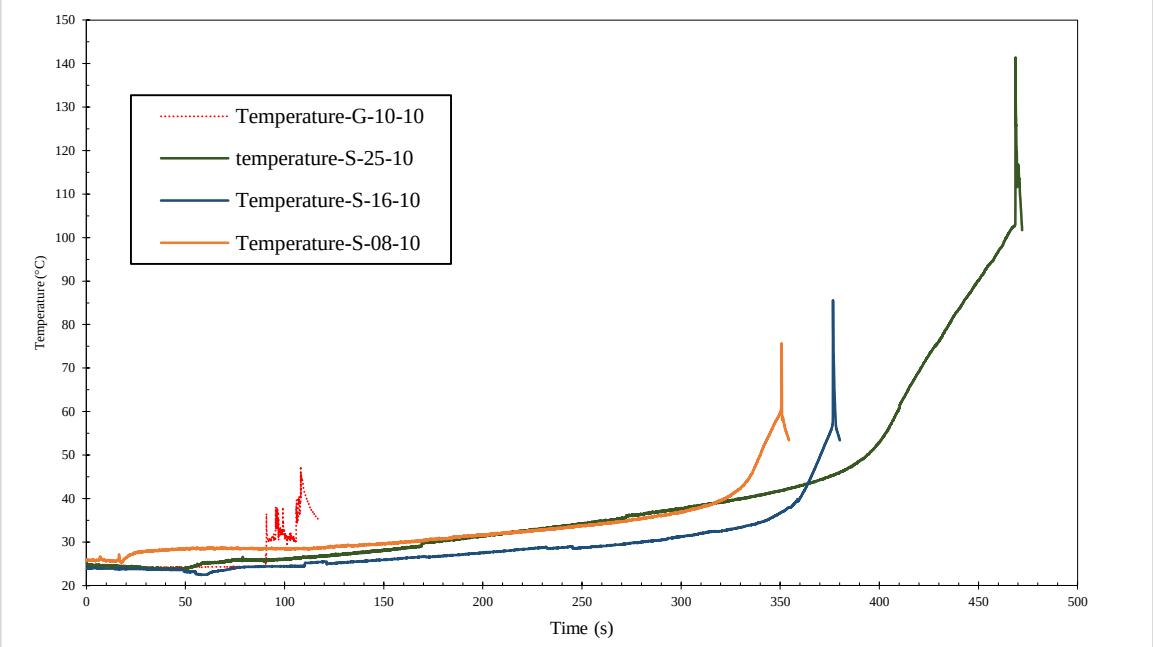

***Figure 18.** Temperature-time curve for steel and GFRP*

Figure 18 shows the thermal behavior of the different bars used in this study under 10 mm/min loading rate, for the curves representing steel it has a smooth curve and this denotes a specific point on the length in the bar, furthermore as observed on the curve representing the FRP the points on the curve are scattered this indicates that the whole length of the bar randomly heats.

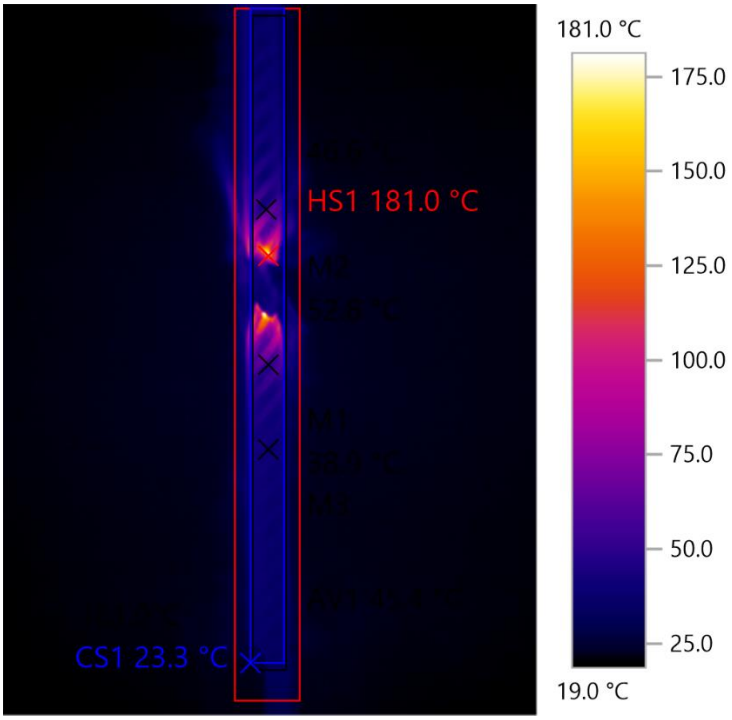

Figure 19. *thermal properties of steel bar at failure 25 mm diameter*

Figure 19 shows a thermograph of a 25 mm bar at failure indicating the hotspot, further details about this can be obtained from the recorded video as well Table 5 shows the meta data of the analyzed image. “M” indicates a point along the length of the specimen “CS” indicates the coldest spot, “HS” indicates the hottest spot and “AV” is the average temperature.

Table 5. *meta data of analyzed steel bar at failure*

No	Temp. [°C]	Emissivity	Reflected Temp. [°C]
M1	52.8	0.60	20.0
M2	46.6	0.60	20.0
M3	38.9	0.60	20.0
CS1	23.3	0.60	20.0
HS1	181.0	0.60	20.0
AV1	45.4	-	-

Table 6. *meta data of analyzed GFRP bar at failure*

No	Temp. [°C]	Emissivity	Reflected Temp. [°C]
M1	31.3	0.80	21.0
M2	31.7	0.80	21.0
M3	39.8	0.80	21.0
CS1	24.1	0.80	21.0
HS1	44.7	0.80	21.0
AV1	30.4		

Figure 20 shows a thermograph of the GFRP at point of failure, and indicates all characteristics points in Table 6 and its behavior the variables stands for the same meaning as described for the table 5. A clear difference between Figure 19 and 20 can be seen from the average temperature within the whole length and the hottest point.

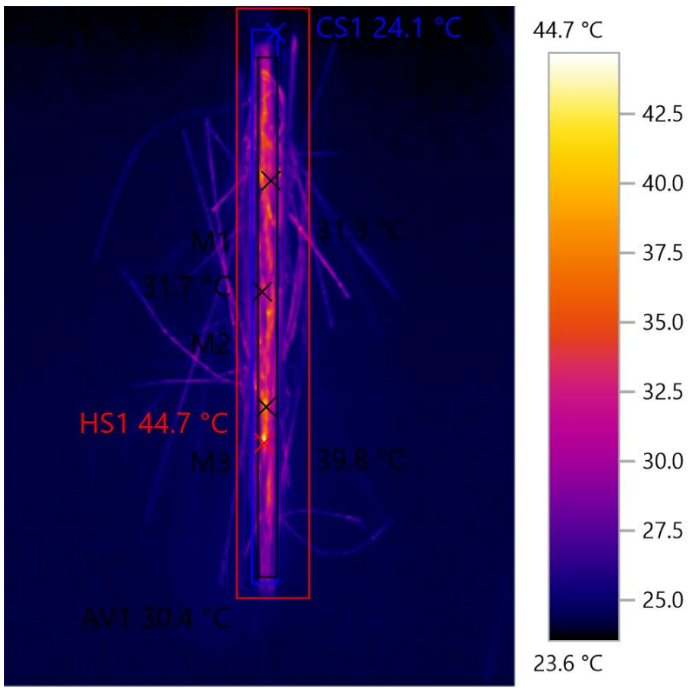

Figure 20. *thermal properties of GFRP bar at failure 10 mm diameter*

5.4 Locating Failure point

Figure 21 shows the temperature changes along the bar at different time interval, as observed the necking point and the breaking point can be spotted from the experiments earlier before failure occurs. The first image was 40 seconds from the start of the experiment and the last where the fracture occurred is 85 seconds.

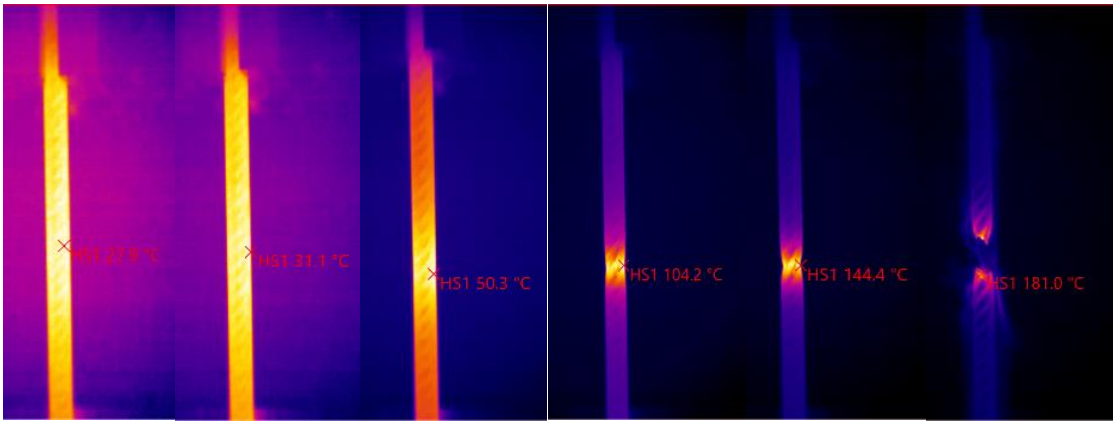

Figure 21*. Identifying failure point of steel bar*

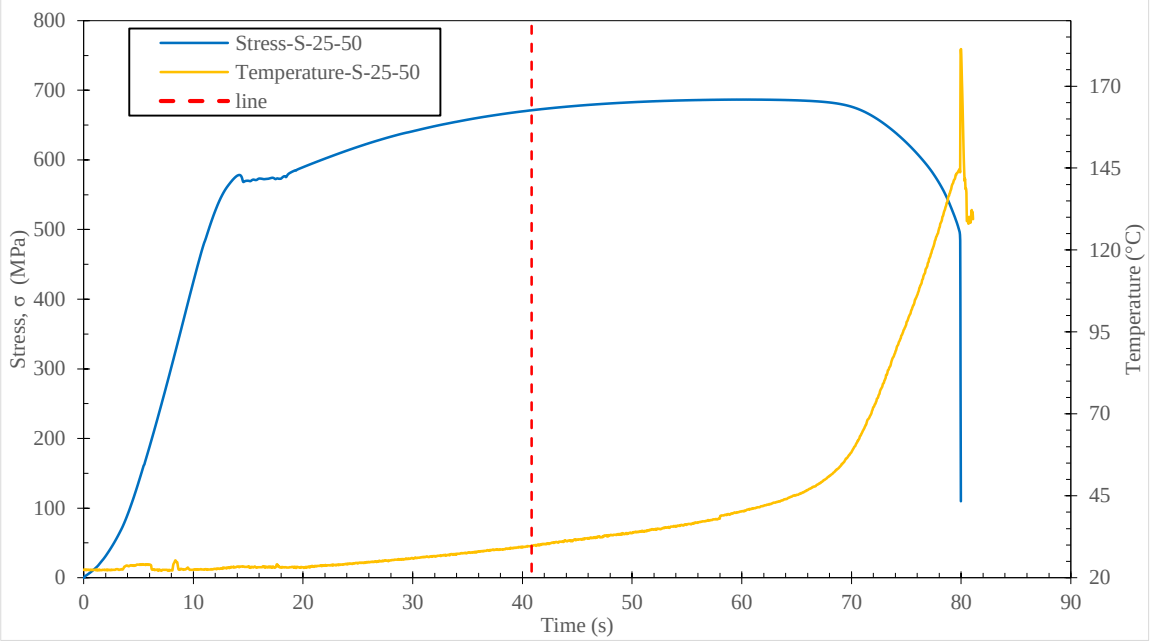

Figure 22. *Tensile test (steel) at 50mm/min displacement rate. Stress-time (left), temperature-time(right)*

Figure 22 shows the stress-time and temperature curve of the experiments illustrated in Figure 21, the red line indicates when the failure point was located, the line intersects with the corresponding stress level and temperature, from the curves it is concluded that using this technique, failure spots can be monitored and can be known half way into the experiment without reaching the maximum tensile stress.

6. CONCLUSIONS

The study aimed to achieve two main objectives: (i) to use the experimental technique of thermography for monitoring temperatures of reinforcement bars during tensile strength test, checking its possibility for this kind of applications; (ii) use the obtained results to analyze the thermal performance of different reinforcement bars with different thicknesses. The steel bars show higher thermal characteristics recording a temperature of up to 181 °C, the GFRP has a reach a high temperature of 47.7°C. Figures in this study shows the mechanical properties of the rebars as well, the steel has a tensile stress of 686 MPa and the GFRP has a tensile stress of 984 MPa and1024 MPa for the two different type (see Figure 4).

Emissivity values of tested specimens have been observed to be higher in rough surfaces. In this case it is the GFRP bar; some of the steel bar have visibly rusty surfaces hence, have a higher Emissivity value than those without rust, information obtained from such experimental technique can be used in future research for accurate non-contact temperature measurement and for heat transfer calculations.

Steel and GFRP bars specimen were tested for strength, and the temperature development was simultaneously monitored by a thermography camera, it is therefore possible to spot the failure point in steel beforehand with this technique.

This technique reveals a strong potential, as the image collected at each instant is in fact a snapshot of the surface temperatures monitored at all the pixels, Such richness of information about the temperature distribution cannot be obtained using other conventional temperature sensors, and therefore the thermography technique has a strong potential for in situ applications.

ACKNOWLEDGEMENT

I express my special gratitude to my research supervisors, Dr. Nagy Balázs, and Dr. Sándor Sólyom for their special guidance and insightful comments, which is greatly invaluable to the completion of this project. The faculty of civil engineering and Budapest university of Technology and Economics for this opportunity.

To my parents Mr. Emmanuel and Mrs. Fatima, am grateful for the spiritual support and everything to this time, you have done all what you are supposed to do. My siblings, Kanwaye, Ahkalola, Catherine and Victor, your encouragement and motivation has always kept me moving; to all my family you are always in my heart thanks for always being there when I needed someone to talk to. My friends and classmates your presence has been a great stir up, motivation, thank you for assisting in any way, thanks for the time spent together.

REFERENCES

[1] R. Pleşu, G. Teodoriu, and G. Ţăranu, “Infrared Thermography Applications for Building Investigation.,” *Apl. Termogfrafierii Cu Infraroşu La Investig. Clădirilor.*, vol. 62, no. 1, pp. 157–168, 2012, [Online]. Available: http://search.ebscohost.com/login.aspx?direct=true&db=a9h&AN=79915036&site=ehost-live.

[2] M. . Clarence Y. Sugihara, M.D., Theodore L. Squier, “The Significance of Tensile and Other Mechanical Test Properties of Metals,” *Proc. Inst. Mech. Eng.*, vol. 151, no. 6, pp. 116–130, 1951.

[3] S. Sólyom, “Bond behaviour of FRP bars to concrete, influence of bar surface, entrained air and high temperatures,” p. 184, 2021.

[4] M. Motavalli, C. Czaderski, A. Schumacher, and D. Gsell, *Fibre reinforced polymer composite materials for building and construction*. Woodhead Publishing Limited, 2010.

[5] P. A. Vo Dong, C. Azzaro-Pantel, M. Boix, L. Jacquemin, and S. Domenech, *Modelling of Environmental Impacts and Economic Benefits of Fibre Reinforced Polymers Composite Recycling Pathways*, vol. 37, no. June. Elsevier, 2015.

[6] G. Ma, Y. Huang, F. Aslani, and T. Kim, “Tensile and bonding behaviours of hybridized BFRP–steel bars as concrete reinforcement,” *Constr. Build. Mater.*, vol. 201, pp. 62–71, 2019, doi: 10.1016/j.conbuildmat.2018.12.196.

[7] A. Raza, S. A. R. Shah, H. Alhazmi, M. Abrar, and S. Razzaq, “Strength profile pattern of FRP-reinforced concrete structures: A performance analysis through finite element analysis and empirical modeling technique,” *Polymers (Basel).*, vol. 13, no. 8, 2021, doi: 10.3390/polym13081265.

[8] C. Meola, Ed., *Infrared Thermography Recent Advances and Future Trends*. Bentham Science Publishers, 2012.

[9] P. D. Pastuszak, A. Muc, and M. Barski, “Methods of infrared non-destructive techniques: Review and experimental studies,” *Key Eng. Mater.*, vol. 542, pp. 131–141, 2013, doi: 10.4028/www.scientific.net/KEM.542.131.

[10] NPL, “What is emissivity and why is it important?”

https://www.npl.co.uk/resources/q-a/why-is-emissivity-important (accessed Oct. 21, 2021).

[11] I. Gigahertz-Optik, “II.8. Reflection, Transmission, and Absorption.” https://light-measurement.com/reflection-absorption/ (accessed Oct. 21, 2021).

[12] P. Botsaris and J. Tsanakas, “Infrared thermography as an estimator technique of a photovoltaic module performance via operating temperature measurements,” *Proc. 10th ECNDT Conf.*, no. June, pp. 1–11, 2010, [Online]. Available: http://ndt.net/article/ecndt2010/reports/1_05_17.pdf.

[13] “Thermal Imaging Cameras & Scopes.” https://www.tester.co.uk/thermal-night-vision-optics/thermal-cameras (accessed Oct. 21, 2021).

[14] Testo, “testo 885 - Thermal imager.” https://www.testo.com/en-SE/testo-885/p/0563-0885-X4 (accessed Oct. 21, 2021).

[15] S. Eleftheriadis, P. Duffour, B. Stephenson, and D. Mumovic, “Automated specification of steel reinforcement to support the optimisation of RC floors,” *Autom. Constr.*, vol. 96, no. June, pp. 366–377, 2018, doi: 10.1016/j.autcon.2018.10.005.

[16] ISO 10406-1, “Fibre-reinforced polymer (FRP) reinforcement of concrete - Test methods,” vol. 2015, pp. 1–10, 2015.

[17] S. Provided and I. S. O. No, “INTERNATIONAL STANDARD Steel for the reinforcement of concrete —,” vol. 2012, 2012.

[18] Testo, “testo IRSoft - PC analysis software,” 2021. https://www.testo.com/hu-HU/termekek/termografia-irsoft (accessed Oct. 29, 2021).